Journal of Molecular Liquids 212 (2015) 227–236

Contents lists available at ScienceDirect

Journal of Molecular Liquids

journal homepage: www.elsevier.com/locate/molliq

Synthesis of bimetallic Fe–Zn nanoparticles and its application towards adsorptive removal of carcinogenic dye malachite green and Congo red in water

Ravindra Kumar Gautam [a], Vandani Rawat [a], Sushmita Banerjee [a], Maria Angeles Sanroman [b,*], Shivani Soni [c], Sanjeev K. Singh [d], Mahesh Chandra Chattopadhyaya [a,*]

[a] Environmental Chemistry Research Laboratory, Department of Chemistry, University of Allahabad, Allahabad 211 002, India
[b] Department of Chemical Engineering, Isaac Newton Building (F.F.T.), University of Vigo, Vigo36310, Spain
[c] Department of Biological Sciences, Alabama State University, 915 S Jackson St., Montgomery, AL 36104, United States
[d] Eco-System Division, National Environmental Engineering Research Institute (CSIR), Nehru Marg, Nagpur 440020, India

ARTICLE INFO

Article history:
Received 1 June 2015
Received in revised form 4 September 2015
Accepted 7 September 2015
Available online 20 September 2015

Keywords:
Bimetallic Fe–Zn nanoparticles
Adsorption
Isotherm
Kinetics
Malachite green
Congo red

ABSTRACT

In this study, a novel bimetallic Fe–Zn nanoparticle was synthesized via a coprecipitation method and applied for the adsorptive removal of carcinogenic dye malachite green (MG) and Congo red (CR) in water. The synthesized bimetallic Fe–Zn nanoparticles were characterized by TEM, XRD, FTIR, and SEM with an attached EDX, a BET surface area analyzer, and by determining pH_{zpc}. Batch adsorption experiments were conducted to evaluate the adsorption process by varying the optimization parameters such as the solution pH, time, and initial dye concentration. The process was initially very rapid, and the maximum adsorption was observed within 60 min of contact time. The kinetics of removal were tested with a pseudo-first order, a pseudo-second order, and an intra-particle diffusion model and showed the best agreement with the pseudo-second order model. Adsorption data were modeled with Langmuir, Freundlich, Temkin, and Dubinin–Radushkevich isotherms and had a good fit with the Langmuir isotherm model. The Langmuir maximum adsorption capacity for MG and CR was found to be 21.74 and 28.56 mg/g, respectively. The adsorption process was endothermic with positive values of ΔH° of 62.73 and 69.65 kJ/mol for MG and CR, respectively, and was spontaneous, as the ΔG° value was negative for all of the samples. A positive ΔS° value indicates increased disorder at the solid–solution interface during the adsorption of the MG and CR dyes. An attempt was made to regenerate the MG- and CR-loaded bimetallic Fe–Zn nanoparticles with suitable eluents and the regenerated bimetallic Fe–Zn nanoparticles were reused seven and six times with removal levels higher than 70% for the adsorption of MG and CR, respectively.

1. Introduction

The release of colored wastewater into nearby bodies of water brings about great harm to aquatic animals and plants because dyes and their by-products alter the water chemistry. Colored wastewater interferes with the transmission of sunlight into streams and reduces photosynthetic activity [1], which results in the gradual destruction and disruption of aquatic ecosystems [2]. Moreover, dyes can cause severe health disorders in human beings and affect the function of kidneys, the reproductive system, the liver, the brain, and the central nervous system and might be carcinogenic, mutagenic, or allergenic to aquatic life [3]. Hence, an urgent need to treat dye-containing wastewater effluents prior to discharge into nearby bodies of water exists. Several physicochemical methods such as cloud point extraction [4–7], membrane filtration, and adsorption [2,8] have been tested to remove pollutants from industrial effluents; many of these methods have their own advantages and disadvantages. Activated carbon adsorption has become popular to remove dyes because of cost, the relative simplicity of the design, ease of operation and insensitivity to toxic substances. However, the high cost of activated carbon limits the application of this technique on an industrial scale in most developing countries. Hence, a growing interest to find a cost effective material for the removal of hazardous dyes from wastewater exists.

Recently, zerovalent metallic iron (Fe^0) and magnetic nanoparticles have been successfully utilized to remove dyestuffs from aqueous media due to their low cost, high efficiency, ease of operation, effectiveness, and biocompatibility with nature [9–11]. Gautam et al. [8] have reviewed various remedial methods for pollutant removal. Iron oxidized organic compounds can remediate a variety of contaminants when used in the presence of oxygen [12]. Fan et al. [9] used nanoscale zerovalent iron particles to decolorize methyl orange in aqueous solution with a decolourization efficiency of 100% within 60 min; pH

* Corresponding authors.
E-mail addresses: sanroman@uvigo.es (M.A. Sanroman), mcchattopadhyaya@gmail.com (M.C. Chattopadhyaya).

http://dx.doi.org/10.1016/j.molliq.2015.09.006
0167-7322/

adjustment was unnecessary because of the high surface area, small particle size, and the large density of intrinsic surface sites of the iron particles [13]. The use of nanoscale iron particles has been well established for the separation and purification of toxic metal ions and organic compounds [14]. However, reports indicate that the pollutant adsorption rate by iron oxide nanoparticles was very slow [8,12]. Furthermore, the addition of a second catalytic metal such as Ni, Cu, Pd and Pt might enhance the adsorption rate compared with nanoscale iron alone [15,16] and also prevents oxidation in air. Although various combinations of nanoscale iron-based bimetallic compounds have been utilized for the degradation of phenol, bisphenol A and chlorinated organic compounds [17–20], very few studies exist concerning the removal of dyestuffs from aqueous media. A Fe–Cu bimetallic system was developed for the decolourization of methlyene blue in aqueous solution [21] and the degradation of orange G in aqueous solution was investigated using Fe–Ni bimetallic nanoparticles [22]. Furthermore, the addition of a second metal (Cu, Ni, and Pd) along with iron can produce toxic effects. In addition, the incorporation of Zn with iron enhances the biocompatibility, stability, and adsorption capacity [10]. Yet, bimetallic Fe–Zn nanoparticles have not been utilized for the removal of hazardous dyes so we made an effort to synthesize bimetallic Fe–Zn nanoparticles and utilized them for the adsorption of carcinogenic dyes from wastewater.

Malachite green (MG) and Congo red (CR) were selected as model pollutants because both dyes are associated with carcinogenicity and produce great harm to aquatic biota [23,24]. CR (1-nepthalene sulphonic acid, 3,3′-(4,4′-biphenylenebis(azo))bis(4-amino-)disodium salt) is a benzidine-based anionic azo dye that is known to metabolize benzidine, a human carcinogen [23]. CR has an aromatic structure that provides physicochemical, thermal and optical stability [25]. However, MG is resistant to fading on exposure; when this dye is discharged into water it affects the aquatic life and can cause detrimental effects in the liver, gills, kidney, intestine, gonads, and pituitary gonadotrophic cells [26]. It has been reported that the products formed by MG degradation are also unsafe and potentially carcinogenic [26,27]. Thus, it is necessary to remove such toxic dyes from wastewater before it is discharged into the aquatic environment.

In the present study, novel bimetallic nanoparticles of Fe–Zn oxide were synthesized, characterized, and used as an adsorbent to remove MG and CR from aquatic media. Batch adsorption experiments were conducted using synthetic aqueous solutions of dyes and the effects of the initial dye concentration, the initial solution pH, and temperature were investigated. The kinetics, equilibrium isotherms, and thermodynamics data of the adsorption process were evaluated to elucidate the adsorption mechanism of the dye molecules by the bimetallic nanoparticles of Fe–Zn oxide. An attempt was also made to regenerate and reuse the bimetallic Fe–Zn oxide nanoparticles.

2. Materials and method

2.1. Chemicals

All chemicals were of analytical reagent grade and used as received without further purification. $FeCl_3 \cdot 6H_2O$ (99%), $Zn(NO_3)_2 \cdot 6H_2O$(99.5%), $NaBH_4$ (99.5%), ethanol, and acetone were purchased from Merck, Mumbai, India. NaOH and HCl were from Fisher Scientific. The dyes, Congo red, and malachite green were procured from the British Drug House, Poole, England.

2.2. Method of preparation of bimetallic nanoparticles

The Fe–Zn bimetallic nanoparticles were synthesized using the sodium borohydride ($NaBH_4$) reduction method as reported by Fang et al. [11] with slight modifications. Briefly, deionized water was deoxygenated by purging with N_2 gas for 30 min before use. Then, 0.1 M $FeCl_36H_2O$ was prepared in 100 mL ethanol/water (30/70, v/v). Under nitrogen protection and vigorous stirring, 0.3 M $NaBH_4$ solution was rapidly added to the $FeCl_36H_2O$ solution. The solution was stirred for 10 min, and the stirring was stopped when the mixture turned black. Subsequently, the black particles were magnetically separated. To eliminate excess $NaBH_4$, the synthesized nanoparticles were washed with an excess of deoxygenated water and rinsed with acetone. The reaction can be described by the following equation:

$$2Fe^{2+} + 2H_2O + BH_4^- \rightarrow 2Fe^0 + BO_2^- + 4H^- + 2H_2 \quad (1)$$

To obtain Zn-coated bimetallic nanoparticles, 50 mL ethanol solution was added into the flask to redisperse the freshly prepared nanoscale Fe. Then, 0.1 M $Zn(NO_3)_26H_2O$ in 50 mL ethanol solution was added into the flask. The mixture was stirred for 30 min. The process is represented by the following equation:

$$Fe(s) + Zn^{2+} \rightarrow Fe^{2+} + Zn(s) \quad (2)$$

The washed particles were dried in a hot air oven at 120 °C for 24 h. The dried nanomaterials were crushed to powder, stored in a glass bottle, and used for characterization and adsorption studies.

2.3. Adsorbates

The adsorbate Congo red (CR), an anionic dye with the molecular formula $C_{32}H_{22}N_6Na_2O_6S_2$, C.I. = 22,120 and a λ_{max} = 497 nm and malachite green (MG), a cationic dye with the molecular formula, $C_{23}H_{26}N_2Cl$, C.I. = 42,000 and a λ_{max} = 620 nm, were purchased from the British Drug House, Poole, England (Fig. 1). A stock solution of 500 mg/L of both dyes was prepared and the required concentrations of working dye solutions were prepared by appropriate dilution of the stock solution.

2.4. Analytical measurements

The dye concentration was determined by measuring absorbance using a double beam UV–vis spectrophotometer (Systronics 2202, Ahmadabad, India) and the surface morphology was studied using scanning electron microscopy (FEI Quanta 200 MK2, Japan) at an electron accelerated voltage of 20 kV coupled with an electron dispersive X-rays (EDX) Genesis Software attachments. The X-ray diffraction (XRD) analysis was conducted using a Philips X'pert Pro diffractometer using CuK_α radiation (λ = 1.54060 Å). Transmission electron microscopy (TEM) images of the Fe–Zn nanoparticles were obtained with a Philips CM200 Transmission Electron Microscope, operating at an accelerating voltage of 200 kV. FTIR spectra of the Fe–Zn nanoparticles and dye-loaded nanoparticles were collected with a FTLA-2000 ABB spectrophotometer, Canada in the range 400–4000 cm^{-1}, using a resolution of

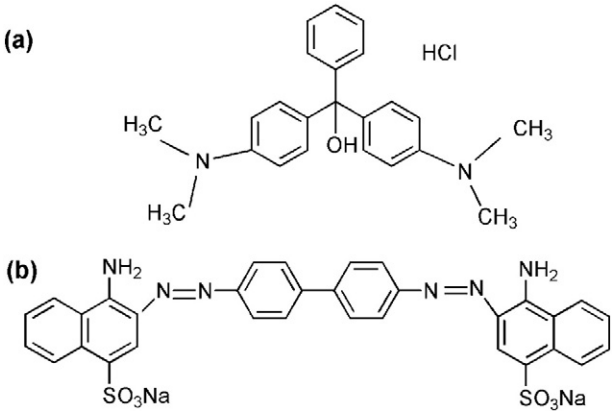

Fig. 1. Chemical structure of MG (a) and CR (b).

4 cm^{-1} and 32 scans to determine the surface functional groups. The spectra of the dried samples were obtained in KBr pellets (Merck, spectroscopic grade) containing 1 wt.% of Fe–Zn nanoparticles. The BET surface area was measured by a N_2 adsorption–desorption isotherm at temperature 77 K using an Autoasorb 1C instrument for BET. The Brunauer–Emmett–Teller (BET) and Barrett–Joyner–Halenda (BJH) methods were used to calculate the surface area of synthesized Fe–Zn nanoparticles. The zeta potential of the bimetallic Fe–Zn nanoparticles was measured at various pH values with a Zeta Probe, Colloidal Dynamics, USA. A digital pH meter (Systronics 335, Ahmadabad, India) was used to measure pH, and a water bath orbital shaker (Shivam ISO 900/2000) was used to shake the solutions.

2.5. Adsorption experiments

Adsorptive removal of MG and CR from aqueous solutions by Fe–Zn bimetallic nanoparticles was performed in batch mode to obtain rate and equilibrium data. The experiments were performed to observe the effect of important parameters such as contact time, pH, temperature, and initial dye concentration. In each adsorption experiment, 50 mL of dye solution of a known concentration was added to 0.15 g of Fe–Zn nanoparticles in a 250 mL Erlenmeyer flask and the mixture was stirred in a thermostatic orbital shaker at 120 rpm. The samples were withdrawn from the shaker at predetermined times and the adsorbent was separated from the solution using an external permanent handheld magnet. The residual dye concentration was determined from absorbance values measured before and after treatment with the Fe–Zn bimetallic nanoparticles at λ_{max} 620 nm for MG and at λ_{max} 497 nm for CR with the double beam UV/Vis spectrophotometer. Experiments were also conducted in a pH range from 2 to 10, which was adjusted by using 0.1 N HCl or 0.1 N NaOH solution to determine the optimum pH for the removal of MG and CR. To investigate the effect of temperature on the adsorption characteristics, studies were conducted at different temperatures in a range 293–323 K. The adsorption capacity (q_t, mg/g) at any time, t, and the dye removal percentage (R%) were calculated using the following equations:

$$q_t = (C_o - C_t)\ V/m \tag{3}$$

$$R\% = (C_0 - C_e) \times (1/C_0) \times 100 \tag{4}$$

where C_o (mg/L) is the initial concentration of the solute in the aqueous solution, C_t (mg/L) is the solute concentration in the aqueous phase at time t, C_e (mg/L) is the equilibrium concentration, V is the volume of the solution (L), and m is the mass of the adsorbent (g).

2.6. Desorption and regeneration studies

The desorption study is very important because the regeneration of the adsorbent determines the economic success of the adsorption process [28]. In the present study, several solvents were used to regenerate the bimetallic nanoparticles. Desorption of MG was performed by placing the MG-sorbed bimetallic nanoparticles into a methanol solution containing 5% acetic acid [29]. The 0.1 M NaOH aqueous solutions were found to be effective to desorb CR from the loaded bimetallic Fe–Zn nanoparticles. A certain amount of dye loaded on 0.15 g of bimetallic Fe–Zn nanoparticles was kept in an Erlenmeyer flask containing 100 mL of the eluent solution and agitated in a water bath shaker. When equilibrium was attained, the nanoparticles were separated with an external handheld permanent magnet and the concentration of the dye in the liquid phase was measured to estimate the amount of dye desorbed. The CR loaded bimetallic nanoparticles were regenerated using an aqueous 0.1 M NaOH solution and the procedure was repeated many times until the CR could not be detected in the solution. Then, the bimetallic nanoparticles were washed thoroughly with distilled water to a neutral pH. The regenerated bimetallic Fe–Zn nanoparticles were reused in subsequent adsorption experiments. The procedure was repeated using the same bimetallic Fe–Zn nanoparticles seven and six times for MG and CR, respectively.

2.7. Replication of batch experiments

Each batch adsorption experiment described above was conducted in triplicate to obtain reproducible results with an error <5%. All of the batch adsorption experimental data in Section 3 (results and discussion) are the average values of three tests. The error functions, Chi square test (χ^2), sum of the square of the error (SSE), and residual root mean square error (RMSE) were calculated across the studied range using the solver add-in with Microsoft's Excel spreadsheet by the following Eqs. (5)–(7) [31]:

$$\chi^2 = \sum_{i=1}^{n} \frac{\left(q_{e,\,cal} - q_{e,\,exp}\right)^2}{q_{e,\,exp}} \tag{5}$$

$$SSE = \sum_{i=1}^{n} \left(q_{e,\,cal} - q_{e,\,exp}\right)_i^2 \tag{6}$$

$$RMSE = \sqrt{\frac{1}{n-2}\sum_{n=1}^{1}\left(q_{e,\,cal} - q_{e,\,exp}\right)^2} \tag{7}$$

where $q_{e,cal}$ and $q_{e,exp}$ refer to the theoretical and experimental capacities (mg/g), respectively, and n is the number of experimental observations.

3. Results and discussion

3.1. Characterization

The physicochemical properties of the bimetallic Fe–Zn nanoparticles were investigated via TEM, SEM-EDX, XRD and BET surface area analysis. SEM analysis confirmed the presence of nanoparticle crystals useful for the determination of the porosity, particle shape, and size. Therefore, the morphology of the nanomaterial was spherical in shape, and the particle size was in the nano range (Fig. 2a). EDX analysis confirmed the presence of iron and zinc oxide (Fig. 2b). A TEM image showed that the bimetallic Fe–Zn nanoparticles were in a range of 15 to 20 nm (Fig. 2c). The XRD results showed the presence of crystalline particles of iron and zinc oxide (Fig. 2d), and a peak at 44.9° corresponded to nano zero valent iron (JCPDS-00-006-0696) with a lattice plane (110). Peaks at 31.75, 34.38, 36.18, 47.50, 56.54, 62.78, 66.31, 67.84, and 68.91° corresponded to zinc oxide (JCPDS-36-1451) with Miller lattice indices of (100), (002), (101), (102), (010), (103), (200), (112), and (201), respectively. The size of the nanoparticles was calculated by Debye–Scherrer's formula [13]. The XRD outcome was consistent with the TEM results, corroborating the high crystallinity of the nanoparticles. The BET surface area was measured by nitrogen adsorption–desorption (Fig. 2e) and was 73.08 m^2/g, whereas the BJH desorption pore size distribution was 21.78–8.88 m^2/g, the total pore volume was 0.2698 cc/g and the average BET pore size was 250.50 Å.

The FTIR spectra of wave numbers ranging from 400 to 4000 cm^{-1} for bare Fe–Zn bimetallic nanoparticles and particles loaded with MG and CR are shown in Fig. 3. Fig. 3a shows the characteristic band at 3200–3600 cm^{-1}, which is attributed to O–H bending vibrations. The band at 1520–1600 cm^{-1} corresponds to C═O, and the band at 1400–1450 cm^{-1} to C═C vibrations [30]. The spectrum of the parent magnetite nanoparticles shows strong peaks at 585 cm^{-1} due to the Fe–O functional group [31] and a slightly weak peak appeared at 1086 cm^{-1} due to C–O stretching [32]. The absorption peak at a lower frequency 550 cm^{-1} can be assigned to the stretching vibrations of the Zn–O bonds in the tetrahedral positions [33]. A similar observation has been reported in the literature by Fu and Wang [34]. The spectra

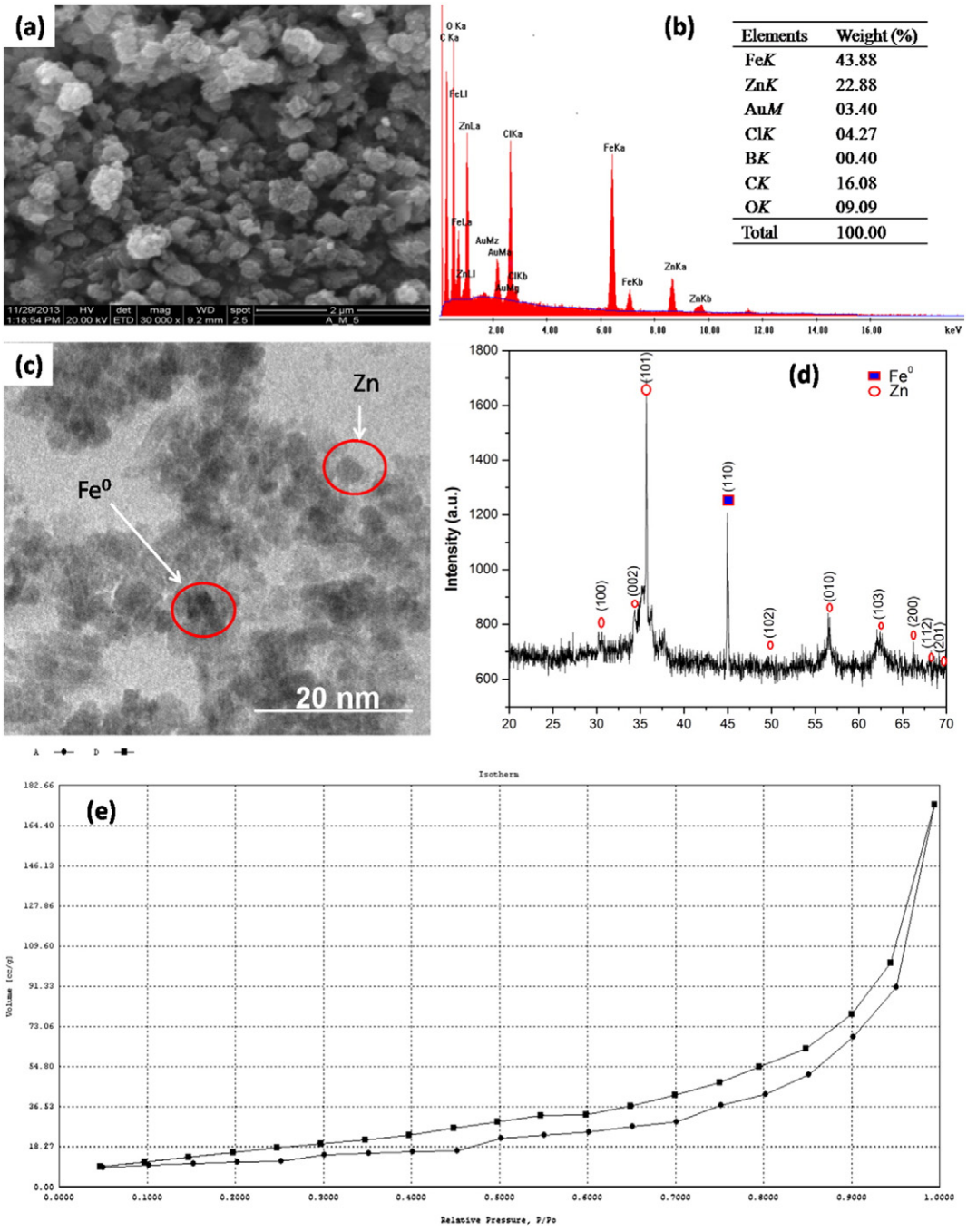

Fig. 2. SEM micrograph (a), EDX spectra with atomic weight percentage (b), TEM image (c), XRD spectra (d), and the N_2 adsorption–desorption graph (e) of the bimetallic Fe–Zn nanoparticles.

of Fe–Zn bimetallic nanoparticles loaded with MG and CR were also measured (Fig. 3b and c) and clearly showed that after the adsorption of MG and CR, there was a slight change in the peaks.

3.2. Effect of contact time and the initial dye concentration

The influence of the initial dye concentration and the effect of the contact time on dye removal were investigated using 25, 50, 75, and 100 mg/L solutions of MG and CR at various contact times. The results reveal that rapid adsorption of MG and CR dyes occurred initially and the removal rate gradually decreased thereafter until equilibrium was reached (Fig. 4). The rapid adsorption is a result of an abundance of active sites on the adsorbent surface in the initial stage of contact. As time passes, the active sites are occupied by dye molecules so the rate of adsorption declines.

An evaluation of the effect of initial dye concentration led to the conclusion that for a low initial dye concentration, the percent removal is high and increasing the dye concentration rapidly decreases the percent removal. The maximum percent removal was 92% for MG and 98% for CR at 25 mg/L of dye. However, the net uptake of dye is higher at a higher dye concentration in solution compared with a low concentration of dye in solution because of an increase in the driving force for the mass transfer.

3.3. Effect of solution pH

The zeta potential of the bimetallic Fe–Zn nanoparticles as-prepared was measured at various pH values and the pH_{zpc} was found to be ~7.4. The effect of pH on the removal of MG and CR was evaluated over a pH range from 2 to 10 and the results are shown in Fig. 5. For MG,

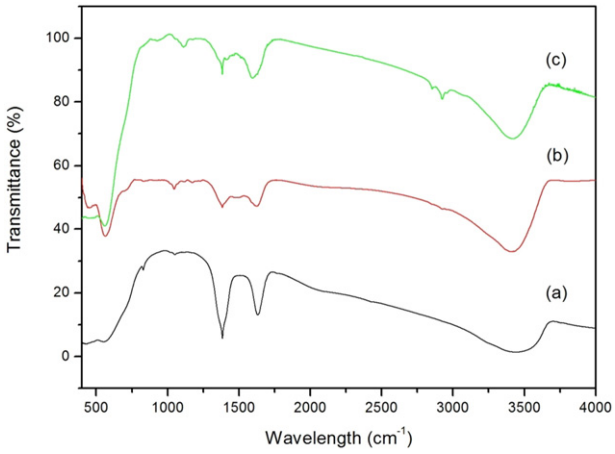

Fig. 3. FTIR spectra of the bimetallic Fe–Zn nanoparticles (a), bimetallic Fe–Zn nanoparticles loaded with CR (b) and MG (c).

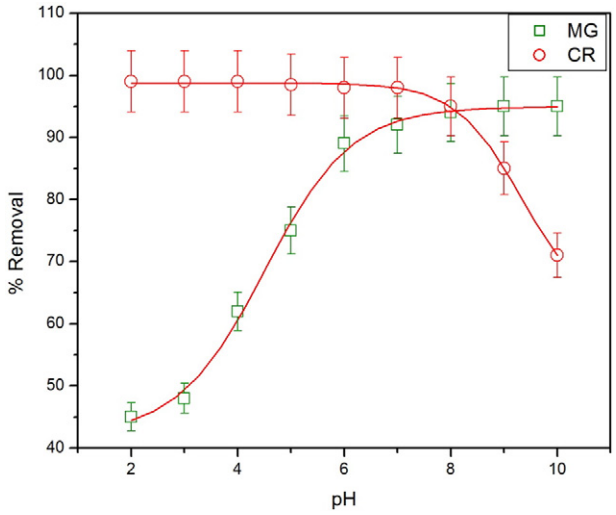

Fig. 5. Effect of pH on the removal of MG and CR (initial dye concentration = 25 mg/L, agitation speed = 120 rpm, adsorbent dose = 0.15 g, contact time = 60 min, temperature = 303 K).

when solution pH > pH_{zpc}, the surface of adsorbent was negatively charged and the adsorption of MG was favored. With an increase in pH, the adsorption of MG increased rapidly. At pH 9.0, the maximum adsorption was found to be 95% through the electrostatic interaction between adsorbent functional groups and the cationic dye, which can be further corroborated by the pH_{zpc} (~7.4) of the adsorbent. When the solution pH is acidic, the H^+ ions compete with positively charged MG ions for the adsorption sites of the nanoadsorbents, forming MGH^{+2} species [35]. Hence, only a very small amount of removal of MG by the bimetallic nanoparticles was evident. A similar result was observed by Tang et al. [36] for the adsorption of MG on a chitin hydrogel.

The maximum removal of CR was 99% at pH ~4.0 within a 60 min contact time at 25 mg/L dye. Subsequent lowering of solution pH ~2.0 did not affect the removal of CR, which was at equilibrium at 99%. When the pH was increased from 2 to 10, the adsorption of CR decreased rapidly from 99% to 71% due to the repulsion between the dye and negatively charged surface of the bimetallic nanoparticles. The pH_{zpc} of nanoparticles was ~7.4, which means that above the pH_{zpc}, the surface was negatively charged and repulsion occurred, and below the pH_{zpc}, the surface of the adsorbent was positively charged so it favored the adsorption of the anionic CR dye. Similar results were reported by Namasivayam and Kavitha [37] for the removal of CR by activated carbon prepared from coir pith.

3.4. Adsorption kinetic modeling

Experimental data were fit to various kinetic models such as pseudo-first order, pseudo-second order, and intra-particle diffusion models. The pseudo-first order rate equation can be expressed as [38]:

$$\ln(q_e - q_t) = \ln q_e - k_1 t \quad (8)$$

where q_e (mg/g) and q_t (mg/g) are the amount of adsorbed adsorbate at equilibrium and at time t, respectively, and k_1 (min^{-1}) is the rate constant of pseudo-first order adsorption. The slope and intercept of the plot of log (q_e–q_t) versus t are used to determine the pseudo-first order rate constant, k_1. The correlation coefficient (R^2) was low (Table 1) and a very large difference existed between q_e (experimental) and q_e (calculated) for the pseudo-first order model. In addition, the theoretical and experimental equilibrium adsorption capacities, q_e, obtained from this kinetic model varied greatly at all concentrations. The inapplicability of the pseudo-first order model to describe the kinetics of pollutants by adsorption using the adsorbents has also been observed in previous studies [31,39–41].

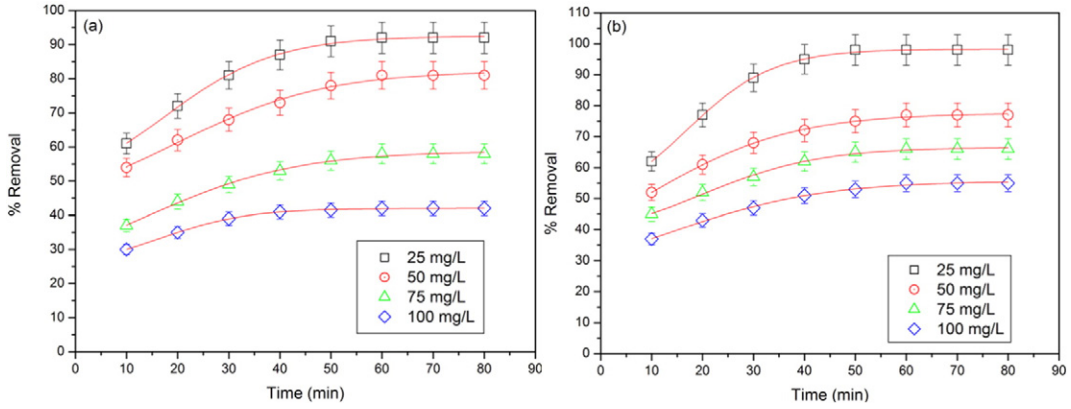

Fig. 4. Effect of time on the removal of MG (a) and CR (b) by the bimetallic Fe–Zn nanoparticles (temperature = 303 K, adsorbent dose = 0.15 g, solution pH = 7, agitation speed = 120 rpm).

Table 1
Kinetic parameters for the adsorption process of MG and CR on Fe–Zn bimetallic nanoparticles.

Pseudo-first order							
MG concentration (mg/L)	$q_{e,exp}$ (mg/g)	k_1 (1/min)	$q_{e,cal}$ (mg/g)	R^2	χ^2	SSE	RMSE
25	11.50	0.082	11.98	0.930	0.020	0.230	0.479
50	20.25	0.064	17.46	0.938	0.384	7.784	2.789
75	21.75	0.058	13.71	0.987	2.972	64.641	8.039
100	21.00	0.083	15.85	0.977	1.262	26.522	5.149
CR concentration (mg/L)	$q_{e,exp}$ (mg/g)	k_1 (1/min)	$q_{e,cal}$ (mg/g)	R^2	χ^2	SSE	RMSE
25	12.25	0.082	11.61	0.981	0.033	0.409	0.639
50	19.25	0.062	13.14	0.981	1.939	37.332	6.109
75	24.75	0.073	21.62	0.928	0.395	9.796	3.129
100	27.50	0.069	31.94	0.986	0.716	19.713	4.439
Pseudo-second order							
MG concentration (mg/L)	$q_{e,exp}$ (mg/g)	k_2 (g/mg/min)	$q_{e,cal}$ (mg/g)	R^2	χ^2	SSE	RMSE
25	11.50	0.0093	13.15	0.998	0.236	2.722	1.649
50	20.25	0.0051	22.72	0.997	0.301	6.100	2.469
75	21.75	0.0042	25.00	0.997	0.485	10.562	3.249
100	21.00	0.0058	24.39	0.996	0.547	11.492	3.389
CR concentration (mg/L)	$q_{e,exp}$ (mg/g)	k_2 (g/mg/min)	$q_{e,cal}$ (mg/g)	R^2	χ^2	SSE	RMSE
25	12.25	0.016	12.30	0.989	0.0001	0.002	0.044
50	19.25	0.025	17.24	0.967	0.209	4.040	2.009
75	24.75	0.018	22.22	0.971	0.258	6.400	2.529
100	27.50	0.015	25.00	0.980	0.227	6.250	2.500

The pseudo-second order model is expressed by [42]:

$$\frac{dq_t}{dt} = k_2(q_e - q_t)^2. \tag{9}$$

Rearranging the variables gives,

$$\frac{dq_t}{(q_e - q_t)^2} = k_2 dt. \tag{10}$$

Integrating this equation for the boundary conditions $t = 0$ to $t = t$ and $q = 0$ to $q = q_t$, gives:

$$\frac{t}{q_t} = \frac{1}{(k_2 q_e^2)} + \frac{t}{q_e} \tag{11}$$

where k_2 (g/mg/min) is the equilibrium rate constant of the pseudo-second order adsorption. The slope and intercept of the plot of t/q_t versus t were used to calculate the second-order rate constant, k_2. The corresponding kinetic parameters for these models are listed in Table 1. The R^2 for the pseudo-second order adsorption model is high (>0.99), consequently plots of t/q_t against t at different concentrations showed excellent linearity. The calculated equilibrium adsorption capacity (q_e^{cal}) was consistent with the experimental equilibrium adsorption capacity (q_e^{exp}) at all dye concentrations (Table 1). These statistical parameters and adsorption capacity results suggested that the pseudo-second order adsorption model was provided a better equation to describe the adsorption kinetics of dye to the Fe–Zn bimetallic nanoparticles. The adsorption of MG on clay also followed pseudo-second order kinetics [24]. Literature reports also indicate that the pseudo-second order kinetic model fitted the adsorption of CR onto the activated carbon well [37,43].

An adsorption process that is characterized by intra-particle diffusion is described by the equation [44]:

$$q_t = k_{id} t^{1/2} + I \tag{12}$$

where k_{id} is the intra-particle diffusion rate constant, and value of I indicates the thickness of the boundary layer, i.e., the larger intercept, the greater the boundary layer effect.

If intra-particle diffusion is involved in the adsorption process, the plot is linear and intra-particle diffusion is the rate-controlling step if the line passes through the origin. If the line does not pass through the origin, it can be inferred that not only intra-particle diffusion but also the boundary layer (film diffusion) influences the rate-controlling step to some degree. Multilinearity indicates that the adsorption process occurs in three principal steps. The first is attributed to the transfer of adsorbate molecules from the bulk solution to the external surface of the adsorbent via diffusion through the boundary layer (film diffusion). The second describes the diffusion of the adsorbate from the external surface into the adsorbent pores (pore or intra-particle diffusion). The final step is the adsorption of the adsorbate on the active sites on the internal surface of the pores. The last step generally occurs rapidly so that the overall adsorption is controlled by either film or pore diffusion, or a combination [3]. An evaluation of intra-particle mass transfer curve of the two dyes at different initial concentrations, confirmed that the plot was multilinear, which indicates that two or more process were involved in the adsorption of the MG and CR dyes. The adsorption process for both dyes (MG and CR) occurred in two distinct phases in — film diffusion (first phase) and intra-particle diffusion (second phase). The intra-particle rate constant and parameters for these dyes are given in Table 2. Comparing the rate constants and the value of I indicates that the line did not pass through the origin; hence, intra-particle diffusion is not the only rate limiting mechanism. Adsorption of MG and CR is a complex process and is controlled by intra-particle diffusion and surface sorption.

3.5. Adsorption isotherm

The adsorption capacity is defined by the adsorption isotherm. Various models have been developed to describe the behavior of adsorbent materials. We considered four different adsorption isotherms – Langmuir, Freundlich, Temkin, and Dubinin–Radushkevich – to correlate the equilibrium adsorption data.

Table 2
Parameters of the intra-particle diffusion model.

	MG			CR		
Dye concentration (mg/L)	K_{id} (mg/g. min$^{1/2}$)	I	R^2	K_{id} (mg/g. min$^{1/2}$)	I	R^2
25	0.778	5.55	0.937	0.921	5.45	0.879
50	1.356	9.46	0.983	1.379	9.00	0.978
75	1.581	9.39	0.970	1.792	11.46	0.985
100	1.171	12.22	0.882	1.766	13.53	0.969

The Langmuir model describes a homogenous and uniform surface of materials that forms a monolayer. The model is based on the assumption that adsorption takes place at specific homogeneous sites within the adsorbent and no interaction occurs between the adsorbed species. The Langmuir isotherm has the following form [45]:

$$q_e = \frac{q_m K_L C_e}{1 + K_L C_e} \tag{13}$$

which may be written in linearized form as follows:

$$\frac{C_e}{q_e} = \frac{1}{q_m K_L} + \frac{C_e}{q_m} \tag{14}$$

where q_m (mg/g) is maximum adsorption capacity of the adsorbent for the dyestuff, C_e (mg/L) is the liquid phase equilibrium concentration of the dyestuff, q_e (mg/g) is the amount of dye adsorbed, and K_L (L/mg) is the constant related to the energy or net enthalpy of adsorption. A plot of C_e/q_e versus C_e should be linear with a slope $1/q_m$ and an intercept of $1/(q_m K_L)$. The values of q_m, K_L, and R^2 obtained from the Langmuir curves are shown in Table 3. The Langmuir maximum adsorption capacity of the bimetallic Fe–Zn nanoparticles was found to be 21.74 and 28.56 mg/g for MG and CR, respectively. As seen from Table 3, the Langmuir isotherm provides the best R^2 and hence best fit for the experimental data. Table 4 provides a comparison of the maximum monolayer adsorption capacities of the MG and CR adsorption on adsorbents from various sources.

The Freundlich equation has the following form [46]:

$$q_e = K_F C_e^{1/n} \tag{15}$$

The linear form may be written as:

$$\ln q_e = \ln K_F + \frac{1}{n} \ln C_e \tag{16}$$

where q_e (mg/g) is the amount of dye adsorbed, C_e (mg/L) is the liquid phase equilibrium concentration of the dyestuff, K_F (mg/g) can be taken as a relative indicator of the adsorption capacity, and $1/n$ is the indicative of the energy or the intensity of the reaction. The Freundlich isotherm constant n indicates the favorability of the adsorption process — the value of n should be less than 10 and more than unity for favorable adsorption conditions. Table 3 shows that the values of n are in the range of 1 to 10 for MG and CR. Similar results have been reported by Gautam et al. [2] for the adsorption of Alizarin Red S from aqueous solutions by mustard husks.

Table 3
Isotherm parameters for the adsorption of MG and CR by the Fe–Zn bimetallic nanoparticles.

Isotherm model	MG	CR
Langmuir		
q_m (mg/g)	21.74	28.56
K_L (L/mg)	0.14	0.32
R^2	0.999	0.994
Freundlich		
K_F (mg/g)	11.59	13.56
n	6.06	5.917
R^2	0.749	0.979
Temkin		
K_T (L/mg)	11,047.9	729,416.3
B	0.228	0.305
b (J/mol)	11,048.8	8259.48
R^2	0.759	0.953
D–R		
q_{DR} (mg/g)	21.24	23.45
γ (mol^2/kJ^2)	6×10^{-7}	8×10^{-8}
E (kJ/mol)	10.00	17.85
R^2	0.959	0.830

Table 4
Adsorption capacities for sorption of MG and CR dyes onto various adsorbents.

Adsorbents	Adsorption capacity (mg/g)	References
MG		
Activated carbon of *Borassus aethiopum*	4.47–48.48	Nethaji et al. [51]
Activated carbon of rice husk	56.497–92.592	Rahman et al. [52]
Bagasse fly ash	170.00	Mall et al. [23]
Banana pseudo-stem fiber	26.50	Gupta et al. [53]
Bentonite	178.60	Bulut et al. [50]
Chitosan coated bentonite beads	435.00	Ngah et al. [54]
Chitosan bead	93.55	Bekci et al. [55]
Chitin hydrogel	0.092 (mmol/g)	Tang et al. [36]
Chemically modified rice husk	12.16–17.98	Chowdhury et al. [56]
Clayey soil	78.57	Saha et al. [24]
Fe–Zn bimetallic nanoparticles	21.74	Present study
CR		
Activated carbon of coir pith	6.72	Namasivayam and Kavitha [37]
Activated carbon	300.00	Purkait et al. [43]
Chitosan hydrobeads	92.59	Chatterjee et al. [57]
Coal-based mesoporous activated carbon	52–189	Lorenc-Grabowska and Gryglewicz [58]
Kaolin	5.44	Vimonses et al. [59]
Bentonite	35.84	Vimonses et al. [59]
Zeolite	3.77	Vimonses et al. [59]
Magnetic nanoparticles ($MnFe_2O_4$)	41.99	Liu et al. [60]
Fe–Zn bimetallic nanoparticles	28.56	Present study

The Temkin isotherm contains a factor that explicitly takes adsorbing species–adsorbent interactions into account. This isotherm assumes that the heat of adsorption of all molecules in the layer decreases linearly with coverage due to adsorbate–adsorbent interactions and that the adsorption is characterized by a uniform distribution of binding energy. The equation is in the following form [47]:

$$q_e = {}^{RT}/_{b} \ln(K_T C_e) \tag{17}$$

A linear form of the Temkin isotherm can be expressed as:

$$q_e = B \ln K_T + B \ln C_e \tag{18}$$

where $RT/b = B$. The adsorption data can be analyzed according to Eq. (18); therefore, a plot of q_e versus ln C_e enables the determination of the constants K_T and B. K_T is the equilibrium binding constant (L/mg) corresponding to the maximum binding energy and the constant B is related to the heat of adsorption. The values of the Temkin constant K_T, B, and the R^2 are provided in Table 3. R^2 is lower than that for the Langmuir, Freundlich, and D–R isotherm models. Therefore, the Temkin isotherm is not a good fit for the adsorption process of MG and CR for Fe–Zn nanoparticles.

The Dubinin–Radushkevich (D–R) isotherm model describes the adsorption on both homogeneous and heterogeneous surfaces. It provides an estimation of the characteristic porosity of an adsorbent as well as its apparent energy of adsorption. The model has a linear form as [48]:

$$\ln q_e = \ln q_{DR} - \gamma \varepsilon^2 \tag{19}$$

where q_{DR} is the D–R adsorption capacity (mg/g), γ is the adsorption energy constant (mol^2/kJ^2) and ε is the Polanyi potential, which is defined as:

$$\varepsilon = RT \ln\left(1 + {}^{1}/_{C_e}\right) \tag{20}$$

where R and T are the gas constant (8.314 J/mol/K) and the absolute temperature, respectively. From a linear plot of ln q_e versus ε^2, the

values of γ and q_{DR} were determined by the slope and intercept. The mean sorption energy (E), which is the free energy for the transfer of 1 mol of dye from infinity to surface of the adsorbent can be estimated from the value of γ, as follows:

$$E = \frac{1}{\sqrt{2\gamma}}. \quad (21)$$

The value of E gives information about the type of adsorption mechanism such as chemical ion exchange or physical adsorption. A value of E between 8.0 and 16.0 kJ/mol corresponds to an ion exchange process whereas a value <8.0 kJ/mol represents a physical process [49,50]. In the present study, the values of E were calculated to be between 8.0 and 16.0 kJ/mol (Table 3), which suggests that the ion exchange was the major mechanism responsible for the adsorption of MG and CR onto the bimetallic Fe–Zn nanoparticles.

By comparing the R^2 values of all four isotherm models, it can be concluded that Langmuir isotherm model is the best fit for both of the dyes MG and CR. However, the favorable value of n of the Freundlich isotherm may be due to both a homogeneous and heterogeneous distribution of active sites on the surface of Fe–Zn nanoparticles.

3.6. Thermodynamic study

Thermodynamic studies of the adsorption of MG and CR on the bimetallic Fe–Zn nanoparticles were undertaken to explore the mechanism involved. Different thermodynamic parameters such as the change in the standard free energy (ΔG°), enthalpy (ΔH°), and entropy (ΔS°) were estimated with the following equations [31]:

$$\log K_c = \frac{\Delta S^\circ}{2.303R} - \frac{\Delta H^\circ}{2.303RT} \quad (22)$$

$$\Delta G^\circ = \Delta H^\circ - T\Delta S^\circ \quad (23)$$

where R (8.314 J/mol K) is the gas constant, T (K) is the absolute temperature, and K_c (L/g) is the standard thermodynamic equilibrium constant defined by q_e/C_e. The values of ΔH° and ΔS° were calculated from the slopes and intercepts of a plot of log K_c versus $1/T$. The various thermodynamic parameters at the three temperatures studied are given in Table 5. The values of ΔG° were found to be negative at all temperatures, which indicated that the adsorption process of MG and CR on the active adsorption sites on the Fe–Zn bimetallic nanoparticles was spontaneous [61]. The observed decrease in the value of ΔG° with an increase in temperature suggested that a higher temperature would facilitate the adsorption of dyes onto the Fe–Zn bimetallic nanoparticles. A similar observation was made by Tang et al. [36] who studied the adsorption of MG on chitin hydrogels in aqueous solution. A positive value of ΔH° indicated that the process is endothermic because an increase in temperature increases the rate of diffusion of the adsorbate molecules across the external boundary layer and the internal pores of adsorbent particles, consequently decreasing the viscosity of the aqueous solution. The positive value of ΔS° shows increased disorder at the solid–solution interface during the adsorption of MG and CR dyes on the Fe–Zn bimetallic nanoparticles.

The nature of sorption process that dominates the sorption behavior of dye onto Fe–Zn bimetallic nanoparticles were also investigated and the activation energy (E_a) was determined through the Arrhenius expression given as:

$$\ln k_2 = \ln A - (E_a/RT) \quad (24)$$

where k_2 is pseudo-second order rate constant (g/mg/min), E_a is the activation energy (kJ/mol), R is the universal gas constant (8.314 J/mol K), and T is the absolute temperature (K). The slope of linear plot of ln k_2 versus $1/T$ can be used for the estimation of E_a and the results of the same are depicted in Table 5. The value of the E_a provides information related to the type of sorption process, for physisorption process E_a value is usually <40 kJ/mol, while value >40 kJ/mol indicates chemisorption as the dominant process. In this study, the E_a values for the adsorption of MG and CR onto the bimetallic Fe–Zn nanoparticles were found to be 40.83 and 42.66 kJ/mol, respectively, which is greater than 40 kJ/mol and this undoubtedly recommends the involvement of chemical forces in sorption process.

3.7. Effect of recycling adsorbents on dye adsorption

A desorption study was conducted to explore the possibility of recycling the Fe–Zn bimetallic nanoparticles. Desorption of MG from MG-sorbed nanoparticles was performed in methanol containing 5% acetic acid solution as the eluent [29]. About a 95.0% adsorption efficiency was achieved when 5% (v/v) acetic acid was used in methanol solution (Fig. 6). This result was similar to that reported in the literature [29].

Desorption of CR from Fe–Zn bimetallic nanoparticles was demonstrated using three different eluents: 0.01 M NaOH, 0.1 M NaOH, and 0.5 M NaOH. The quantitative desorption efficiencies were determined to be 82.6%, 96.3% and 88.0%, respectively. The reusability was checked by following the adsorption–desorption process for the three eluents. The 0.1 M NaOH solution was the optimum eluent. It has been reported in the literature that 0.1 M NaOH was a suitable eluent for desorption of the acidic dye tartrazine from tartrazine loaded activated carbon [39]. The effect of the recycling time on the adsorption process was assessed by repeating the experiment seven times, and the results are shown in Fig. 6. Fig. 6 indicates that the uptake capacity of CR on the Fe–Zn bimetallic nanoparticles adsorbent decreased slowly as the cycle number increased. The percentage adsorption remained steady at approximately 85% for the first four cycles, and then the uptake capacity of CR decreased. At the sixth regeneration cycle, the adsorption remained at 71.0%. These results show that the Fe–Zn bimetallic nanoparticles can be recycled for CR molecule adsorption with 0.1 M NaOH, and the Fe–Zn bimetallic nanoparticles can be reused. This possibly occurs because, in the basic solution, the positively charged groups were deprotonated and the electrostatic interaction between the adsorbent surface and the CR dye molecules became much weaker [39]. Therefore, the Fe–Zn bimetallic nanoparticles can be reused seven and six times for the adsorption of MG and CR, respectively.

4. Conclusions

Bimetallic Fe–Zn nanoparticles were found to be suitable for the removal of MG and CR molecules from aqueous solution. Adsorption of MG and CR was found to increase with increasing contact time and an increase in the initial dye concentration and in the solution temperature. The adsorption of dye onto bimetallic Fe–Zn nanoparticles was

Table 5
Thermodynamic parameters for the removal of MG and CR onto Fe–Zn bimetallic nanoparticles.

Temperature (K)	MG				CR			
	ΔG° (kJ/mol)	ΔH° (kJ/mol)	ΔS° (J/mol/K)	E_a (kJ/mol)	ΔG° (kJ/mol)	ΔH° (kJ/mol)	ΔS° (J/mol/K)	E_a (kJ/mol)
293	−2.728	62.730	222.645	40.83	−5.010	69.650	255.16	42.66
303	−4.405				−8.056			
313	−7.234				−10.148			

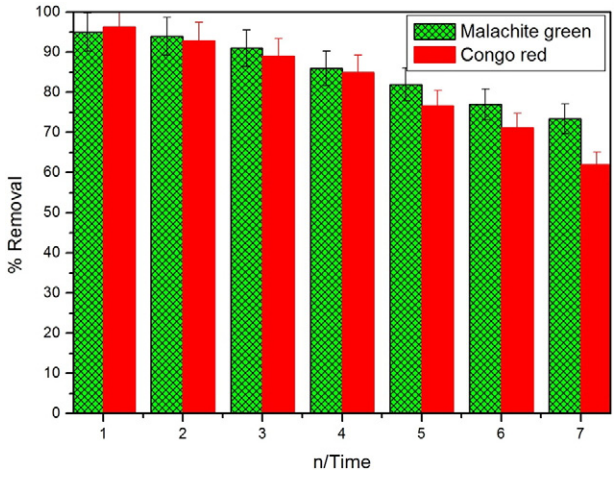

Fig. 6. Effect of recycling Fe–Zn bimetallic nanoparticles on the MG and CR adsorption (temperature = 303 K, agitation speed = 120 rpm, contact time = 60 min, solution pH MG = 9, solution pH CR = 4).

also found to be highly dependent on solution pH and the maximum removal of MG and CR occurred at pH 9 and 4, respectively. The Langmuir isotherm model was well described by the equilibrium data; thus, monolayer adsorption of dye molecules occurred over the bimetallic Fe–Zn nanoparticles. A pseudo-second order kinetic model fit the kinetic data well. It was found that intra-particle diffusion was not the only rate limiting mechanism — the adsorption of MG and CR is a complex process and controlled by both the intra-particle diffusion and surface sorption. The activation energy revealed that the adsorption process was chemically controlled by an ion-exchange mechanism. In thermodynamic studies, the negative value of ΔG° and positive value of ΔH° indicated that the adsorption of MG and CR onto bimetallic Fe–Zn nanoparticles was spontaneous and endothermic. Thus, a higher removal of MG and CR dye molecules could be obtained at a higher temperature. Furthermore, changes in the peaks of the FTIR spectra clearly showed the adsorption of MG and CR dyes on the bimetallic Fe–Zn nanoparticles. The regeneration of MG and CR loaded bimetallic Fe–Zn nanoparticles can be accomplished in methanol containing 5% acetic acid and 0.1 M NaOH as eluents, respectively. The regenerated Fe–Zn bimetallic nanoparticles can be reused seven and six times with removal higher than 70% for the adsorption of MG and CR, respectively, by using the same Fe–Zn bimetallic nanoparticles.

Acknowledgments

R.K. Gautam and S. Banerjee are thankful to the University Grants Commission (UGC) and CSIR—New Delhi, respectively, for the award of Senior Research Fellowship. V.R. is grateful to the University of Allahabad for providing the research fellowship. We are thankful to Prof. S. Basu, Department of Chemical Engineering, Indian Institute of Technology Delhi for providing characterization facilities of SEM-EDX, XRD, and BET. We are also thankful to SAIF, IIT Roorkee for recording TEM micrographs. The authors equally acknowledge the support and provision of the necessary facilities by University of Allahabad, Allahabad, India and the University of Vigo, Vigo, Spain. The support and encouragement of the Prof. V.S. Tripathi from the Department of Chemistry, University of Allahabad are also appreciated.

References

[1] M. Roosta, M. Ghaedi, A. Daneshfar, R. Sahraei, Experimental design based response surface methodology optimization of ultrasonic assisted adsorption of safaranin O by tin sulfide nanoparticle loaded on activated carbon, Spectrochim. Acta, Part A 122 (2014) 223–231.
[2] R.K. Gautam, A. Mudhoo, M.C. Chattopadhyaya, Kinetic, equilibrium, thermodynamic studies and spectroscopic analysis of Alizarin Red S removal by adsorption onto mustard husk, J. Environ. Chem. Eng. 1 (2013) 1283–1291.
[3] C. Duran, D. Ozdes, A. Gundogdu, H.B. Senturk, Kinetic and isotherm analysis of basic dyes adsorption onto almond shell as a low cost adsorbent, J. Chem. Eng. Data 56 (2011) 2136–2147.
[4] M. Soylak, E. Yilmaz, M. Ghaedi, M. Montazerozohori, M. Sheibani, Cloud point extraction and flame atomic absorption spectrometry determination of lead (II) in environmental and food samples, J. AOAC Int. 95 (2012) 1797–1802.
[5] O. Espergham, M. Ghaedi, K. Niknam, S.N. Kokhdan, A cloud point extraction methodology for the determination of trace amounts of copper, cobalt, zinc and manganese by flame atomic absorption spectrometry using a new imidazole derivative, Fresenius Environ. Bull. 20 (2011) 2350–2356.
[6] M. Ghaedi, K. Niknam, E. Niknam, M. Soylak, Application of cloud point extraction for copper, nickel, zinc and iron ions in environmental samples, J. Chin. Chem. Soc. 56 (2009) 981–986.
[7] M. Ghaedi, A. Shokrollahi, K. Niknam, E. Niknam, A. Najibi, M. Soylak, Cloud point extraction and flame atomic absorption spectrometric determination of cadmium(II), lead(II), palladium(II) and silver(I) in environmental samples, J. Hazard. Mater. 168 (2009) 1022–1027.
[8] R.K. Gautam, A. Mudhoo, G. Lofrano, M.C. Chattopadhyaya, Biomass-derived biosorbents for metal ions sequestration: Adsorbent modification and activation methods and adsorbent regeneration, J. Environ. Chem. Eng. 2 (2014) 239–259.
[9] J. Fan, Y. Guo, J. Wang, M. Fan, Rapid decolorization of azo dye methyl orange in aqueous solution by nanoscale zerovalent iron particles, J. Hazard. Mater. 166 (2009) 904–910.
[10] J. Hu, I.M.C. Lo, G. Chen, Comparative study of various magnetic nanoparticles for Cr(VI) removal, Sep. Purif. Technol. 56 (2007) 249–256.
[11] Z. Fang, X. Qiu, J. Chen, X. Qiu, Debromination of polybrominated diphenyl ethers by Ni/Fe bimetallic nanoparticles: Influencing factors, kinetics, and mechanism, J. Hazard. Mater. 185 (2011) 958–969.
[12] S.H. Joo, A.J. Faitz, D.L. Sedleck, T.D. Waite, Quantification of the oxidizing capacity of nanoparticulate zero valent iron, Ind. Environ. Sci. Technol. 39 (2005) 1263–1268.
[13] J.T. Nurmi, P.G. Tratnyek, V. Sarathy, D.R. Baer, J.E. Amonette, K. Pecher, C. Wang, J.C. Linehan, D.W. Matson, R.L. Penn, M.D. Driessen, Characterization and properties of metallic iron nanoparticles: Spectroscopy, electrochemistry, and kinetics, Environ. Sci. Technol. 39 (2005) 1221–1230.
[14] R.K. Gautam, A. Jaiswal, M.C. Chattopadhyaya, Functionalized magnetic nanoparticles for heavy metal removal from aqueous solutions: Kinetics and equilibrium modeling, in: A. Tiwari, M. Syvajarvi (Eds.), Advanced Materials for Agriculture, Food, and Environmental Safety, WILEY-Scrivener Publishing LLC, Massachusetts 2014, pp. 291–331.
[15] J. Wang, P. Blowers, J. Farell, Understanding reduction of carbon tetrachloride at nickel surfaces, Environ. Sci. Technol. 38 (2004) 1576–1581.
[16] B. Schrick, J.L. Blough, A.D. Jones, T.E. Mallouk, Hydrodechlorination of trichloroethylene to hydrocarbons using bimetallic nickel-iron nanoparticles, Chem. Mater. 14 (2002) 5140–5147.
[17] H. Lee, H.Y. Yoo, J. Choi, I.H. Nam, S. Lee, S. Lee, J.H. Kim, C. Lee, J. Lee, Oxidizing capacity of periodate activated with iron-based bimetallic nanoparticles, Environ. Sci. Technol. 48 (2014) 8086–8093.
[18] F. He, D. Zhao, Preparation and characterization of a new class of starch-stabilized bimetallic nanoparticles for degradation of chlorinated hydrocarbons in wáter, Environ. Sci. Technol. 39 (2005) 3314–3320.
[19] C.J. Lin, S.L. Lo, Y.H. Liou, Dechlorination of trichloroethylene in aqueous solution by noble metal-modified iron, J. Hazard. Mater. B116 (2004) 219–228.
[20] X. Wang, C. Chen, Y. Chang, H. Liu, Dechlorination of chlorinated methanes by Pd/Fe bimetallic nanoparticles, J. Hazard. Mater. 161 (2009) 815–823.
[21] L.M. Ma, Z.G. Ding, T.Y. Gao, R.F. Zhou, W.Y. Xu, J. Liu, Discoloration of methlene blue and wastewater from a plant by a Fe/Cu bimatellic system, Chemosphere 55 (2004) 1207–1212.
[22] A.D. Bokare, R.C. Chikate, C.V. Rode, K.M. Paknikar, Effect of surface chemical of Fe–Ni nanoparticle on mechanistic pathway of azo dye degradation, Environ. Sci. Technol. 41 (2007) 7437–7443.
[23] I.D. Mall, V.C. Srivastava, N.K. Agarwal, I.M. Mishra, Adsorptive removal of malachite green dye from aqueous solution by bagasse fly ash and activated carbon-kinetic study and equilibrium isotherm analyses, Colloids Surf. A 264 (2005) 17–28.
[24] P. Saha, S. Chowdhury, S. Gupta, I. Kumar, Insight into adsorption equilibrium, kinetics and thermodynamics of Malachite Green onto clayey soil of Indian origin, Chem. Eng. J. 165 (2010) 874–882.
[25] A. Afkhami, R. Moosavi, Adsorptive removal of congo red, a carcinogenic textile dye, from aqueous solutions by maghemite nanoparticles, J. Hazard. Mater. 174 (2010) 398–403.
[26] S. Srivastava, R. Sinha, D. Roy, Toxicological effect of Malachite green, Aquat. Toxicol. 66 (2004) 319–1329.
[27] S. Singh, M. Das, S.K. Khanna, Biodegradation of malachite green and rhodamine B by cecal microflora and rats, Biochem. Biophys. Res. 200 (1994) 1544–1550.
[28] L. Fan, Y. Zhang, X. Li, C. Luo, F. Lu, H. Qiu, Removal of alizarin red from water environment using magnetic chitosan with alizarin red as imprinted molecules, Colloids Surf. B 91 (2012) 250–257.
[29] A.Z.M. Badruddoza, G.S.S. Hazel, K. Hidajat, M.S. Uddin, Synthesis of carboxymethyl-β-cyclodextrin conjugated magnetic nano-adsorbent for removal of methylene blue, Colloids Surf. A 367 (2010) 85–95.
[30] H.Y. Zhu, R. Jiang, L. Xiao, W. Li, A novel magnetically separable γ-Fe_2O_3/crosslinked chitosan adsorbent: Preparation, characterization and adsorption application for removal of hazardous azo dye, J. Hazard. Mater. 179 (2010) 251–257.

[31] R.K. Gautam, P.K. Gautam, S. Banerjee, S. Soni, S.K. Singh, M.C. Chattopadhyaya, Removal of Ni(II) by magnetic nanoparticles, J. Mol. Liq. 204 (2015) 60–69.
[32] Y. Lin, Z. Chen, M. Megharaj, R. Naidu, Degradation of scarlet 4BS in aqueous solution using bimetallic Fe/Ni nanoparticles, J. Colloid Interface Sci. 381 (2012) 30–35.
[33] G.L. Fan, Z.J. Gu, L. Yang, F. Li, Nanocrystalline zinc ferrite photocatalysts formed using the colloid mill and hydrothermal technique, Chem. Eng. J. 155 (2009) 534–541.
[34] Y. Fu, X. Wang, Magnetically separable $ZnFe_2O_4$ graphene catalyst and its high photocatalytic performance under visible light irradiation, Ind. Eng. Chem. Res. 50 (2011) 7210–7218.
[35] B. Samiey, A. Toosi, Adsorption of malachite green on silica gel: Effects of NaCl, pH and 2 propanol, J. Hazard. Mater. 184 (2010) 739–745.
[36] H. Tang, W. Zhou, L. Zhang, Adsorption isotherms and kinetics studies of malachite green on chitin hydrogels, J. Hazard. Mater. 209–210 (2012) 218–225.
[37] C. Namasivayam, D. Kavitha, Removal of congo red from water by adsorption onto activated carbon prepared from coir pith, an agricultural solid waste, Dyes Pigm. 54 (2002) 47–58.
[38] S. Lagergren, Zur theorie der sogenannten adsorption gelöster stoffe, K. Sven, Vetenskapsakad. Handl. 24 (1898) 1–39.
[39] R.K. Gautam, P.K. Gautam, S. Banerjee, V. Rawat, S. Soni, S.K. Sharma, M.C. Chattopadhyaya, Removal of tartrazine by activated carbon biosorbents of *Lantana camara*: Kinetics, equilibrium modeling and spectroscopic analysis, J. Environ. Chem. Eng. 3 (2015) 79–88.
[40] M. Ghaedi, A. Ansari, M.H. Habibi, A.R. Asghari, Removal of malachite green from aqueous solution by zinc oxide nanoparticle loaded on activated carbon: Kinetics and isotherm study, J. Ind. Eng. Chem. 20 (2014) 17–28.
[41] M. Roosta, M. Ghaedi, A. Daneshfar, R. Sahraei, A. Asghari, Optimization of the ultrasonic assisted removal of methylene blue by gold nanoparticles loaded on activated carbon using experimental design methodology, Ultrason. Sonochem. 21 (2014) 242–252.
[42] Y.S. Ho, G. McKay, Pseudo-second order model for sorption processes, Process Biochem. 34 (1999) 451–465.
[43] M.K. Purkait, A. Maiti, S. DasGupta, S. De, Removal of congo red using activated carbon and its regeneration, J. Hazard. Mater. 145 (2007) 287–295.
[44] W.J. Weber Jr., J.C. Morris, Kinetics of adsorption on carbon from solution, J. Sanit. Eng. Div. ASCE 89 (1963) 31–60.
[45] I. Langmuir, The adsorption of gases on plane surfaces of glass, mica and platinum, J. Am. Chem. Soc. 40 (1918) 1361–1403.
[46] H.M.F. Freundlich, Uber die adsorption in lasugen, J. Phys. Chem. 57 (1906) 385–470.
[47] M.J. Temkin, V. Pyzhev, Recent modifications to Langmuir isotherms, Acta Physchim. USSR 12 (1940) 217–222.
[48] M.M. Dubinin, The potential theory of adsorption of gases and vapors for adsorbents with energetically non-uniform surfaces, Chem. Rev. 60 (1960) 931–937.
[49] T.S. Anirudhan, P.S. Sumithra, Equilibrium, kinetic and thermodynamic modeling for the adsorption of heavy metals onto chemically modified hydrotalcite, Ind. J. Chem. Technol. 17 (2010) 247–259.
[50] E. Bulut, M. Ozacar, I.A. Sengil, Adsorption of malachite green onto bentonite: Equilibrium and kinetic studies and process design, Microporous Mesoporous Mater. 115 (2008) 234–246.
[51] S. Nethaji, A. Sivasamy, G. Thennarasu, S. Saravanan, Adsorption of malachite green dye onto activated carbon derived from *Borassus aethiopum* flower biomass, J. Hazard. Mater. 181 (2010) 271–280.
[52] I.A. Rahman, B. Saad, S. Shaidan, E.S. Sya Rizal, Adsorption characteristics of malachite green on activated carbon derived from rice husks produced by chemical–thermal process, Bioresour. Technol. 96 (2005) 1578–1583.
[53] N. Gupta, A.K. Kushwaha, M.C. Chattopadhyaya, Kinetics and thermodynamics of malachite green adsorption on banana pseudo-stem fibers, J. Chem. Pharm. Res. 3 (2011) 284–296.
[54] W.S.W. Ngah, N.F.M. Ariff, A. Hashim, M.A.K.M. Hanafiah, Malachite green adsorption onto chitosan coated bentonite beads: Isotherms, kinetics and mechanism, Clean – Soil, Air, Water 38 (2010) 394–400.
[55] Z. Bekci, C. Ozveri, Y. Seki, K. Yurdakoc, Sorption of malachite green on chitosan beads, J. Hazard. Mater. 154 (2008) 254–261.
[56] S. Chowdhury, R. Mishra, P. Saha, P. Kushwaha, Adsorption thermodynamics, kinetics and isosteric heat of adsorption of malachite green onto chemically modified rice husk, Desalination 265 (2011) 159–168.
[57] S. Chatterjee, S. Chatterjee, B.P. Chatterjee, A.K. Guha, Adsorptive removal of congo red, a carcinogenic textile dye by chitosan hydrobeads: Binding mechanism, equilibrium and kinetics, Colloids Surf. A 299 (2007) 146–152.
[58] E. Lorenc-Grabowska, G. Gryglewicz, Adsorption characteristics of Congo Red on coal-based mesoporous activated carbon, Dyes Pigm. 74 (2007) 34–40.
[59] V. Vimonses, S. Lei, B. Jin, C.W.K. Chow, C. Saint, Kinetic study and equilibrium isotherm analysis of congo red adsorption by clay materials, Chem. Eng. J. 148 (2009) 354–364.
[60] X. Liu, Z. Zhang, W. Shi, Y. Zhang, S. An, L. Zhang, Adsorbing properties of magnetic nanoparticles Mn-ferrites on removal of congo red from aqueous solution, J. Dispersion Sci. Technol. 36 (2015) 462–470.
[61] R. Jain, V.K. Gupta, S. Sikarwar, Adsorption and desorption studies on hazardous dye Naphthol Yellow S, J. Hazard. Mater. 182 (2010) 749–756.